Effect of Synthesis Parameters on the Chromium Content and Catalytic Activities of Mesoporous Cr−MSU-*x* Prepared under Acidic Conditions

Licheng Liu,[†,‡] Huiquan Li,*[,†] and Yi Zhang[†]

Institute of Process Engineering, Chinese Academy of Sciences, P.O. Box 353, Beijing, 100080, P.R. China, and Graduate University of Chinese Academy of Sciences, Beijing, 100049, P.R. China

Received: March 27, 2006; In Final Form: May 27, 2006

A series of chromium-incorporated MSU-*x* mesoporous molecular sieves were synthesized under different templates, initial Si/Cr molar ratios, aging times, and temperatures in acid solution. The synthesis was performed by using sodium silicate, chromium nitrate, and nonionic poly(ethylene oxide) surfactant as the source of silicone, metal, and the template, respectively. The Cr−MSU-*x* products were analyzed by inductively couple plasma−optical emission spectrometry to determine the actual Cr content and were characterized by X-ray diffraction, N_2 adsorption−desorption, scanning electron microscopy, high-resolution transmission electron microscopy, diffuse reflectance UV−visible, X-ray adsorption near-edge spectroscopy, and temperature-programmed reduction techniques. The Cr species were mostly formed as Cr(VI) in tetrahedral coordination. Two kinds of Cr(VI) species with different reduction abilities were distinguished. The catalytic activities of Cr−MSU-*x* in the dehydrogenation of ethane to ethylene with CO_2 were investigated at the same time. The synthesis parameters explored strongly influence the chromium content in Cr−MSU-*x* and, subsequently, the catalytic activities. The Cr−MSU-*x* synthesized with Si/Cr = 20, aging at 25 °C for 22 h, and templating by fatty alcohol polyoxyethylene ether gave the best activities, resulting in 58.0% ethane conversion and 92.1% ethylene selectivity. The Cr species in Cr−MSU-x are more efficient in activating and converting ethane molecules than are conventional catalysts.

Introduction

Mesoporous silicate molecular sieves (MSMS) possess a diverse range of pores with uniform pore diameters in the 2−50 nm range and a high surface area above 1000 m^2/g, and thus show strong application potential in heterogeneous catalysis.[1] However, these MSMS exhibit very low activity when directly used as catalysts because they possess weak acidity and lack necessary redox abilities.[2] Many efforts have been made to the modification of MSMS to obtain porous materials with more extensive capabilities. The introduction of heteroatoms into the framework of MSMS is an important modification technique, through which MSMS are endowed with either strong acidity or required oxidative ability. Up to now, a variety of heteroatoms have been reported to incorporate into the framework of MSMS such as Al, Ti, V, Zr, Fe, Co, Cr, Zn, Mn, and so forth.[3] Among them, Cr is a very important catalytic component for a lot of chemical reactions, especially in the dehydrogenation of alkanes.[4]

The mesoporous MSU-*x* family is assembled through a neutral route N^0I^0 and exhibits three-dimensional wormlike channels that favor the diffusion of molecular objects. The poly(ethylene oxide) (PEO) templates used in the synthesis of MSU-*x* are low-cost, nontoxic, and biodegradable.[1,5,6] Thus, studies of chromium introduced into MSU-*x* would be valuable for developing Cr-based dehydrogenation catalysts with desirable catalytic activities. In our previous investigation, Cr−MSU-*x* was synthesized and exhibited good performance in the oxidative dehydrogenation (ODH) of ethane to ethylene with CO_2.[7]

It is well-known that the dispersion, the oxidation state, and the structure features of supported species may strongly affect the activity of catalysts. For metallosilicate, metal content, which is influenced by synthesis conditions such as aging time and temperature, has a large impact on the dispersion and oxidation state of supported metal species. However, investigations about the effect of synthesis conditions on metal content and, subsequently, their catalytic activities are scarcely performed.[8] In the present contribution, we describe the synthesis of Cr−MSU-*x* molecular sieves with different templates, initial Si/Cr molar ratios, aging times, and temperatures. The synthesis of Cr−MSU-*x* was carried out under acidic conditions since the low polycondensation rate of silica at low pH tends to produce MSU-*x* of high quality. The Cr content determined by inductively coupled plasma−optical emission spectrometry (ICP−OES) and the catalytic activities detected by the ODH of ethane to ethylene with CO_2 are correlatively studied.

Experimental Section

Synthesis. Two commercially available PEO surfactants—fatty alcohol polyoxyethylene ether ($A(EO)_9$) and poly(ethylene glycol) cotyl-phenyl ether (Triton X-100)—were used to assemble Cr−MSU-*x* metallosilicates. Cr−MSU-1 and Cr−MSU-2, as designated, were prepared from $A(EO)_9$ and Triton X-100 surfactant, respectively. A typical synthesis procedure using $A(EO)_9$ as the template was carried out as follows:

An acidified $A(EO)_9$ solution was prepared by resolving 2.26 g of surfactant in 60 mL of 0.5 mol/L aqueous HCl at 50−60

* Corresponding author. E-mail: hqli@home.ipe.ac.cn. Tel: +86-10-62655828.
† Institute of Process Engineering.
‡ Graduate University.

10.1021/jp061875o CCC: $33.50
Published on Web 07/18/2006

TABLE 1: Physicochemical Properties of Mesoporous Cr−MSU-*x* Prepared under Different Conditions

sample	no.	Si/Cr	t^a (h)	T^b (°C)	d_{100} (nm)	S_{BET} (m^2/g)	$d_{pore}{}^c$ (nm)	V^d (cm^3/g)	$\theta_{wall}{}^e$ (nm)	Cr wt %^{f}
MSU-1	0		22	**25**	4.51	964	2.57	0.62	1.94	
Cr−MSU-1	1	**20**	22	**25**	4.75	941	2.70	0.63	2.05	0.75
	2	**50**	**22**	25	4.51	965	2.64	0.53	1.87	0.40
	3	**100**	22	25	3.97	966	1.97	0.48	2.00	0.22
	4	50	**48**	25	4.61	1028	2.30	0.59	2.31	0.34
	5	50	**4**	25	4.70	961	2.76	0.66	1.94	0.73
	6	20	22	**60**						0.37
	7	20	22	**90**						0.08
Cr−MSU-2	8	**20**	22	25	3.93	935	2.17	0.51	1.76	0.86
	9	**50**	22	25	3.85	1101	2.15	0.59	1.70	0.62
	10	**100**	22	25	3.78	1333	2.12	0.71	1.66	0.49

[a] Aging time. [b] Aging temperature. [c] Pore diameter. [d] Pore volume. [e] Wall thickness. [f] Cr content.

°C. A desired amount of the chromium precursor $Cr(NO_3)_3 \cdot 9H_2O$ was then dissolved in the surfactant solution. The resulting solution of $A(EO)_9$ and $Cr(NO_3)_3$ was then mixed with another solution prepared by dissolving 11.37 g of $Na_2SiO_3 \cdot 9H_2O$ in 100 mL of distilled water under vigorous stirring. The mixed solution was dark-green and nontransparent. The pH value changed from 12−13 to 1.5−2.0, and a jade-green precipitate appeared after the addition of 40 mL of 1 mol/L aqueous HCl to the mixed solution. The resulting sol was stirred moderately at 25 °C for 22 h for aging and crystallization. After separation by filtration, the solid gel was washed with deionized water and dried at 60 °C overnight. The as-synthesized Cr−MSU-*x* was calcined under static air at a heating rate of 2 °C/min up to 600 °C and held for 4 h to remove the template.

The synthesis of Cr−MSU-*x* with Triton X-100 as the template was similar to the above-described $A(EO)_9$ templating process. An acidified Triton X-100 solution was prepared by resolving 2.58 g of Triton X-100 in 60 mL of 0.5 mol/L aqueous HCl at 60 °C. The rest of the procedure was carried out as described above. The molar ratio of Si/surfactant was maintained at 1:0.1.

Owing to the high solubility of Cr cations in acid solution, however, the Cr would not load into Cr−MSU-*x* products entirely. The as-synthesized samples were jade-green and became pale yellow after calcination, indicating that the Cr species in the samples were oxidized to higher oxidation states.

Characterization. X-ray diffraction (XRD) measurements were performed on an X'pert Pro MPD X-ray diffractometer from PANalytical with CuKα radiation ($\lambda = 0.154187$ nm), with generator settings of 40 kV, 30 mA, a scanning speed of 0.017°, and scanning regions at 0.5−6.0°. N_2 adsorption−desorption isotherms were determined with an Autosorb series ASIMP apparatus from Quantachrome. The samples were pretreated at 300 °C under vacuum for 5 h before measurements. Calculation of the specific surface area (Brunauer−Emmett−Teller (BET)), pore volume, and average pore size (Barrett−Joyner−Halenda method) was performed with the software of the apparatus.

The Cr content of Cr−MSU-*x* was analyzed using an OPTIMA 5300DV inductively coupled plasma−optical emission spectrometer from Perkin-Elmer. A known weight of the Cr−MSU-*x* sample was dissolved in the mixture of HF and HNO_3 (3:1 proportion). After complete dissolution, the solution was diluted to the required volume and analyzed for Cr content using the most sensitive wavelength of 267.716 nm.

Scanning electron microscopy (SEM) was performed on a JSM-6700F scanning electron microscope from JEOL. The samples were dispersed in ethanol under ultrasonic conditions, deposited on silver paper, and metallized with gold before measurement. A high-resolution transmission electron microscope (HRTEM) image was obtained from a Hitachi H9000 NAR transmission electronic microscope with an accelerating voltage of 200 kV. The samples were dispersed in ethanol under ultrasonic conditions and deposited on a copper grid before examination.

Diffuse reflectance UV−visible (DR UV−vis) spectroscopic measurements were recorded on a UV2100 spectrometer. The spectra were collected at 200−700 nm referenced to $BaSO_4$. X-ray absorption spectroscopic measurements were performed with synchrotron radiation at the National Synchrotron Radiation Laboratory (NSRL) (Heifei City, China). The synchrotron radiation facility is mainly composed of an 800 MeV electron storage ring with about 100−300 mA of ring current. The data were recorded in X-ray fluorescence mode at room temperature using a Si(111) double-crystal monochromator. The energy step of measurement in the X-ray adsorption near-edge structure (XANES) region was 0.7 eV.

A H_2 temperature-programmed reduction (H_2-TPR) of the catalysts was performed on a CHEMBET3000 chemical adsorption apparatus from Quantachrome using a mixture of 5 vol % H_2/Ar as the reducing gas with a total flow rate of 20 mL/min. A 50 mg sample was heated from room temperature to 800 °C at a heating rate of 10 °C/min after being pretreated at 400 °C for 30 min in He gas flow. The reducing gas was cooled by a mixture of *n*-octane and liquid nitrogen to condense the water generated from reduction of catalyst. The reduction signal was recorded by a thermal conductivity detector (TCD).

The reaction of CO_2 and C_2H_6 was performed at atmospheric pressure in a fixed bed quartz reactor (5.0 mm i.d., 44.0 cm long) at 700 °C. The reactants consisted of $V(CO_2) = 9$ mL/min and $V(C_2H_6) = 3$ mL/min. Catalyst loading was 0.2 g. The products were analyzed on line by a gas chromatograph equipped with a Porapack QS column (3 m, Φ1/4) and a TCD (Shimadzu GC 14B) after reacting for 15 min at a specific temperature.

Results and Discussion

A number of Cr−MSU-*x* samples were synthesized with different templates (designated Cr−MSU-1 for $A(EO)_9$ and Cr−MSU-2 for Triton X-100 as template), initial Si/Cr molar ratios (20, 50, and 100), aging times (4, 22, and 48 h), and aging temperatures (25, 60, and 90 °C). The structure properties and actual Cr content of prepared samples are shown in Table 1.

The actual Cr contents of calcined Cr−MSU-*x* products determined by ICP−OES are listed in the last column in Table 1. The results show that the actual amounts of Cr loaded in Cr−MSU-*x* are much smaller than the amounts added to the

source solution. The high solubility of Cr cations under strong acidic conditions makes it very difficult to incorporate chromium into the framework of MSU-*x*. Chen and Melero discovered the low incorporation of titanium into the framework of SBA-15 in the strong acidity of a gel solution.[8,9] It is very similar to our study for incorporating chromium into MSU-*x*. In addition, synthesis conditions have an obvious influence on Cr content. The actual Cr content decreases gradually with the increase of the initial Si/Cr molar ratio, namely, the decrease of Cr concentration in the source gel solution, for both Cr−MSU-1 (samples 1, 2, and 3) and Cr−MSU-2 (samples 8, 9, and 10). This may be attributed to the fact that higher Cr concentrations add opportunity for more Cr atoms to incorporate into the silicate framework in the polycondensation of silica. It resembles the observation of Arnold that an increase of vanadium in gel resulted in an increase of the vanadium content of the [V]−MCM-41 product.[10] Moreover, longer aging times and higher aging temperatures produce lower Cr content. The decrease in the self-assembling capability of the surfactant leads to incomplete crystallization of mesoporous material at higher temperatures,[11] which may reduce the loading of chromium. The strong acidic conditions would remove chromium from the framework of silica after longer aging times, which enhances the regulation of mesoporous Cr−MSU-*x* (see XRD analysis).

The surface areas (BET) and average pore diameters of different Cr−MSU-*x* samples are in the range of 941−1333 m^2/g and 1.9−2.8 nm, respectively. Some general rules about the influence of reaction conditions on BET surface area and pore diameter seem to hold true. For example, a higher initial Si/Cr ratio results in a higher surface area and a smaller pore diameter (samples 1, 2, and 3 for Cr−MSU-1; samples 8, 9, and 10 for Cr−MSU-2). Cr−MSU-*x* synthesized with a lower initial Si/Cr ratio generally maintains a larger pore diameter and corresponds to higher Cr content (samples 1 and 8). A similar result is observed in sample 5 (relatively high Cr loading, 0.73 wt %), which has a larger pore diameter of 2.76 nm. These results indicate that the introduction of more Cr atoms into the framework of MSU-*x* can widen the pore size. However, the above conclusions are conservative because the pore diameters of Cr−MSU-1 samples are not always larger than that of the MSU-1 sample. Moreover, the results of Chen[8] and Melero[9] show no laws for a change in BET surface area and average pore diameter with reaction conditions. Therefore, some discussions should be carried out carefully. The pore volumes of all samples change within the range of 0.48−0.66 cm^3/g. These structure property data of BET surface area, pore diameter, and pore volume are close to the results of MSU-*x* molecular sieves from other researchers.[1,5,6,12]

Figure 1 shows the XRD patterns of Cr−MSU-*x* with different Si/Cr ratios and aging times. All XRD patterns show one broad peak at about $2\theta = 2°$, corresponding to d_{100} reflections and matching most patterns of MSU-*x* materials reported by different investigators.[5,6] Lower initial Si/Cr ratios and shorter aging times resulted in less intense reflections relative to those at higher Si/Cr ratios and longer aging times, indicating that a lower incorporation of Cr and a longer aging or crystallization time, which also results in a lower incorporation of Cr, favor the formation of high-quality Cr−MSU-*x*. The property differences between $A(EO)_9$ and TX-100 may lead to the different d_{100} spacings of Cr−MSU-1 and Cr−MSU-2. Li et al. synthesized MSU-1 in strong acid media using $A(EO)_9$ as the template, and the d_{100} spacing of all the products were almost above 4.00 nm,[12] while Bagshaw's results showed that [M]−MSU-2 ([M] = Al, Ti, V, and Zr, synthesized by an

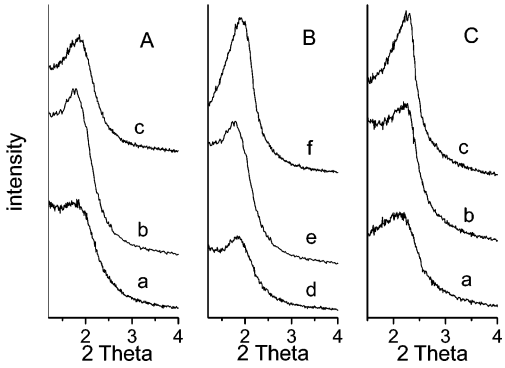

Figure 1. XRD patterns of (A) Cr−MSU-1 and (C) Cr−MSU-2 prepared with different initial Si/Cr ratios: (a) 20, (b) 50, and (c) 100. (B) Cr−MSU-1 with different aging times: (d) 4 h, (e) 22 h, and (f) 48 h.

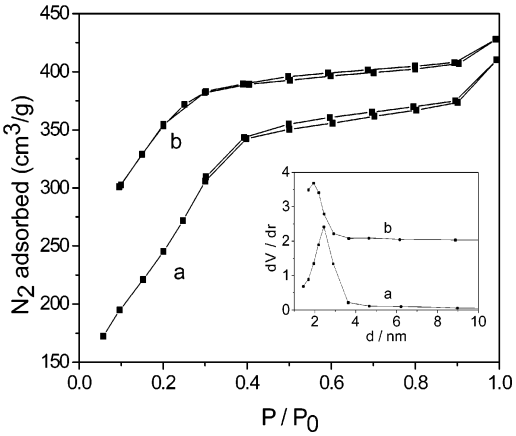

Figure 2. N_2 adsorption−desorption isotherms and pore size distribution curves (inset) of (a) Cr−MSU-1 (sample 1) and (b) Cr−MSU-2 (sample 8).

(alkyl−aryl)−PEO template) always gives d_{100} spacing under 4.1 nm.[1] Because of the longer M−O bond distance than the Si−O bond distance, many authors consider the increase of cell parameter in zeolites[13] as well as in MCM-41[14] as an identification of the presence of metal atoms in the framework of porous material. But in Arnold's opinion,[10] MCM-41 is not a crystalline material, and a change of the repeat distance cannot be directly compared with those of crystalline materials. For example, the T−O bond distance and the T−O−T angle in mesoporous metallosilicate materials have a higher degree of freedom compared with the exactly defined positions in crystalline materials. Our results support Arnold's opinion. The repeat distances of Cr−MSU-1 are not always larger than that of MSU-1. On the basis of the above discussions, the higher degrees of freedom of the system and the larger Cr−O band compared with the Si−O band should both contribute to the subtle difference in the repeat distance in pure silica and chromium-incorporated MSU-*x*.

The N_2 adsorption−desorption isotherms of Cr−MSU-*x* (Cr−MSU-1, sample 1, and Cr−MSU-2, sample 8) are shown in Figure 2. The adsorptions achieve saturation at a relative pressure of $P/P_0 = 0.3-0.4$, and weak hysteresis loops are also observed for both samples, which are typical of structural porous frameworks belonging to type IV isotherms, indicative of the presence of uniform channels.[15,16] Moreover, adsorption of Cr−MSU-1 achieves saturation at a higher relative pressure P/P_0 (∼0.4) than that of Cr−MSU-2 (∼0.3), comparing their N_2 adsorption isotherms shown in Figure 2. This result may be attributed to the larger average pore diameter of Cr−MSU-1

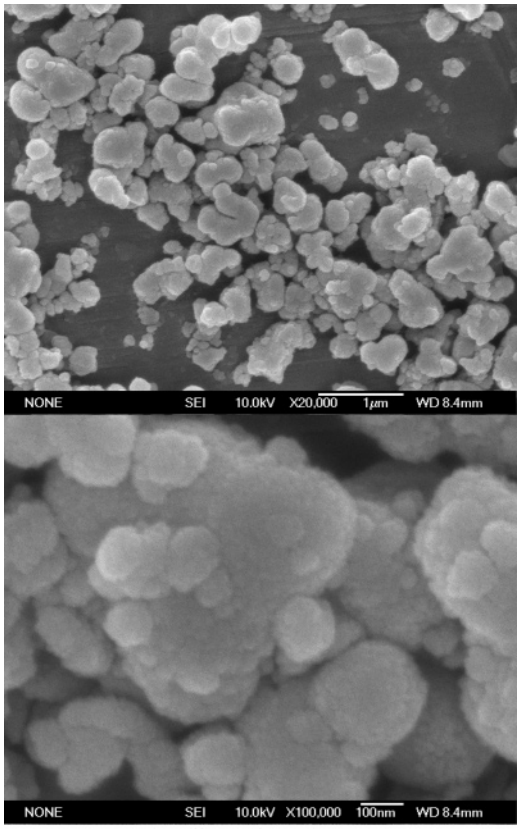

Figure 3. SEM images of calcined Cr−MSU-1 (sample 1).

(2.70 nm) relative to that of Cr−MSU-2 (2.17 nm).[17,18] The regular mesoporous channels are observed from the narrow pore size distribution curves of both samples (Figure 2, inset).

The SEM image of calcined chromium silicate Cr−MSU-1 (sample 1) is shown in Figure 3. Anomalous particle morphologies with particle sizes in the range of 0.1−0.5 μm were observed from the upper SEM micrograph. The lower micrograph with further enlargement shows that the primary particles of average size between 10 and 100 nm are agglomerated to bigger particles. Evidence for the disordered, wormlike packing of channels in Cr−MSU-1 (sample 1) is provided by the two HRTEM images with different enlargements in Figure 4. The average pore diameter estimated from these TEM micrographs agrees well with the results of the N_2 adsorption isotherms.

The oxidation state of Cr species, which has an essential effect on the catalytic activity of Cr-containing catalysts, is investigated in detail. DR UV−vis spectra for Cr−MSU-*x* are given in Figure 5, including samples 1, 2, 5, 6, and 8. Two intense bands centered at 260 and 370 nm, which are usually assigned to O → Cr(VI) charge-transfer absorption, appeared as the main absorption bands for all samples listed in the figure.[19,20] As it is well-known, octahedral Cr(III) species show at least two absorption bands at 450 and 620 nm originating from the $^4A_{2g} \rightarrow {}^4T_{1g}$ and $^4A_{2g} \rightarrow {}^4T_{2g}$ transitions. However, the bands at 450 nm are very weak, and the bands at 620 nm are almost negligible for all samples listed. Therefore, most Cr species in the prepared samples form as Cr(VI) in tetrahedral coordination, indicating that a total oxidation of Cr^{3+} cations occurred during the calcination process.[21] The yellowish color of all the Cr−MSU-*x* samples corresponds to high-valence chromium, which agrees with the above results well. Similar results were observed for Cr−MCM-41.[22,23] Samples 1, 5, and 8 are expected to show more intense bands at 450 nm than the other two samples, suggesting that a certain amount of detectable Cr(III) species

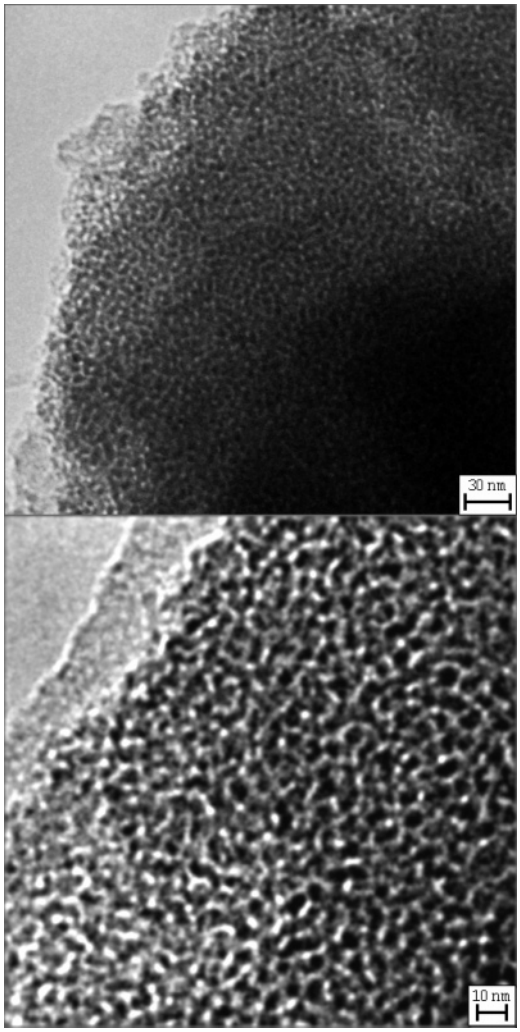

Figure 4. HRTEM images of calcined Cr−MSU-1 (sample 1).

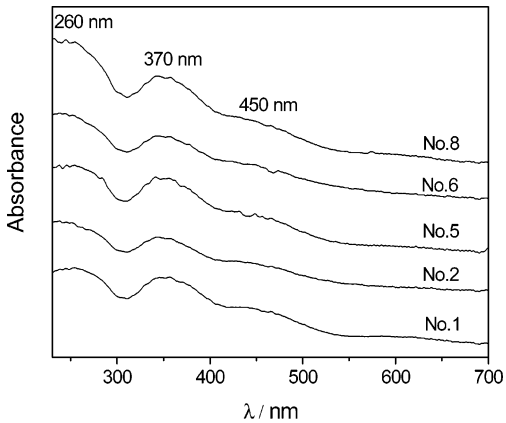

Figure 5. DR UV−vis spectra of Cr−MSU-*x*, including samples 1, 2, 5, 6, and 8.

are formed in the three samples. This may be attributed to the higher Cr contents of 0.75, 0.73, and 0.86 wt % for samples 1, 5, and 8, respectively.

The tetrahedral coordination of Cr atoms in Cr−MSU-*x* is further proved by the Cr K-edge XANES technique. The Cr K-edge XANES spectra of $K_2Cr_2O_7$ and Cr_2O_3 are shown in Figure 6 (curves a and b). A pre-edge peak at ∼5994 eV in the spectra of $K_2Cr_2O_7$ is observed, while no pre-edge peak appears in the spectra of Cr_2O_3. The Cr K-edge XANES spectra of Cr−MSU-1 (sample 1) and Cr−MSU-2 (sample 8) (Figure 6, curves c and d) are similar to that of $K_2Cr_2O_7$. It is well-known that

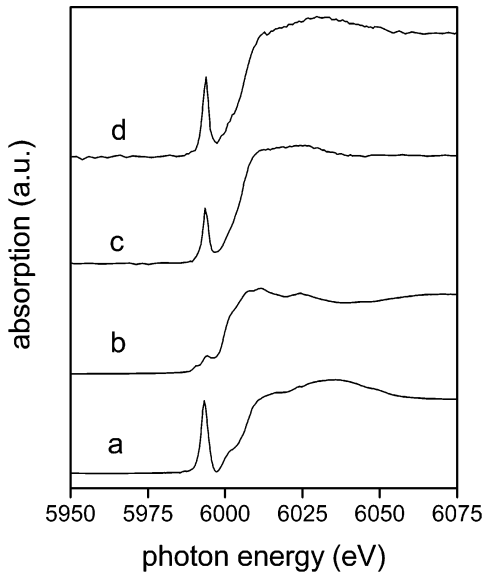

Figure 6. Cr K-edge XANES spectra of (a) $K_2Cr_2O_7$, (b) Cr_2O_3, (c) Cr−MSU-1, (sample 1), and (d) Cr−MSU-2 (sample 8).

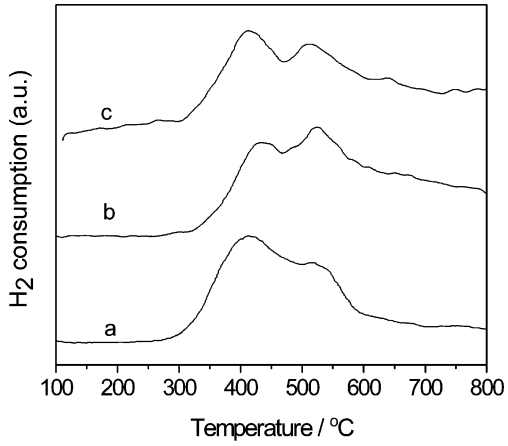

Figure 7. H_2-TPR profiles of (a) Cr−MSU-1 (sample 1), (b) Cr−MSU-1 (sample 5), and (c) Cr−MSU-2 (sample 8).

Cr(VI) atoms in CrO_4^{2-} and CrO_3 present tetrahedral coordination, whereas those in Cr_2O_3 are in octahedral coordination. The 1s−3d transition of Cr atoms is dipole forbidden for octahedral-coordinated compounds such as Cr_2O_3 because of an inversion center. This dipole-forbidden transition is permitted when the Cr center is of noncentral symmetry or the 3d and 4p orbitals are mixing. Therefore, the intensity of the pre-edge peak remarkably increases as the local symmetry around the Cr center changes from octahedral to tetrahedral coordination.[22−24] As a result, a pre-edge peak can be observed in the Cr K-edge XANES spectra of CrO_4^{2-} (Na_2CrO_4, K_2CrO_4) and CrO_3, while no pre-edge peak appears in the spectra of Cr_2O_3.[25−27] It is also concluded that Cr species in Cr−MSU-*x* mostly form as Cr-(VI) in tetrahedral coordination. The XANES technique has been an effective tool to discriminate O_h and T_d site symmetry for transition metal compounds.

Three representative H_2-TPR profiles of Cr−MSU-*x* are shown in Figure 7. They give similar H_2 consumption curves: the reduction began from about 300 °C, and two reduction peaks appear in the process. These peaks are assigned to the reduction of $Cr^{6+} \rightarrow Cr^{3+}$.[23] Two overlapped peaks centered at about 410 and 520 °C for each sample are supposed to originate from the reduction of Cr^{6+} species in and out of the framework, respectively. The Cr^{6+} species out of the MSU-*x* framework,

SCHEME 1: Chemical Structure of Isolated Chromate on the Surface (a) and Incorporated Chromium in the Framework (b) of MSU-*x*

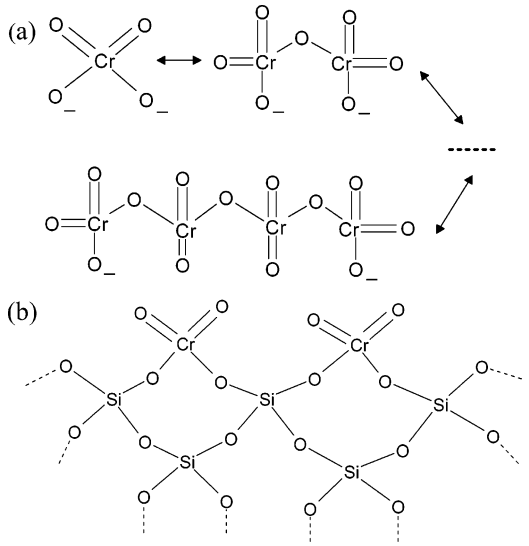

isolated mono- or polychromate, as shown in Scheme 1a, are reduced at lower temperatures. The reduction peak at higher temperatures corresponds to Cr^{6+} species in the framework of MSU-*x*, which interact with the silica support, as shown in Scheme 1b. DR UV−vis spectra and XANES characterization have confirmed Cr^{6+} in tetrahedral coordination, but it is an average result, and Cr species in and out of the MSU-*x* framework cannot be distinguished. H_2-TPR results prove the presence of Cr^{6+} and differentiate two kinds of Cr species with different reduction abilities. The result of two reduction peaks in H_2-TPR treatment is not observed in conventional supported Cr catalysts.[28] The H_2-TPR curves in Figure 7 were treated with a Gaussian fit to distinguish between the different reduction peaks, and the fitting results are listed in Table 2. The area ratios between the two peaks of the three samples are in the following sequence: sample 1> sample 8> sample 5, indicating that more isolated CrO_4 chromates are formed on the inner and outer surface for sample 1, and more incorporated CrO_4 species interact with the silica support for sample 5.

The catalytic activities of Cr−MSU-*x* samples synthesized under different conditions in the dehydrogenation of ethane to ethylene with CO_2 were investigated. The reaction product mainly consists of ethylene, methane, hydrogen, and carbon monoxide. On the basis of the product distribution and reaction pathways proposed by other researchers,[29,30] the following reactions are assumed to take place:

$$C_2H_6 \rightarrow C_2H_4 + H_2 \quad (1)$$

$$CO_2 + H_2 \rightarrow H_2O + CO \quad (2)$$

$$CO_2 + C_2H_6 \rightarrow C_2H_4 + H_2O + CO \quad (3)$$

$$C_2H_6 + H_2 \rightarrow 2CH_4 \quad (4)$$

$$C_2H_6 + 2CO_2 \rightarrow 4CO + 3H_2 \quad (5)$$

The ethylene was produced by the direct dehydrogenation of ethane (reaction 1) and the dehydrogenation of ethane with CO_2 (reaction 3), which could also be seen as the summation of reactions 1 and 2. CO_2 plays the role of a soft oxidant and promotes ethane dehydrogenation. The hydrogenolysis of ethane

TABLE 2: Gaussian Curve Fitting Results with Binary Peaks for the TPR Profiles of Samples 1, 5, and 8

sample no.	T_{max} (°C) P_1[a]	T_{max} (°C) P_2[b]	area ratio P_1/P_2
1	409.9	523.4	2.14
5	423.4	520.6	0.94
8	408.7	512.8	1.90

[a] P_1: reduction peak at lower temperatures. [b] P_2: reduction peak at higher temperatures.

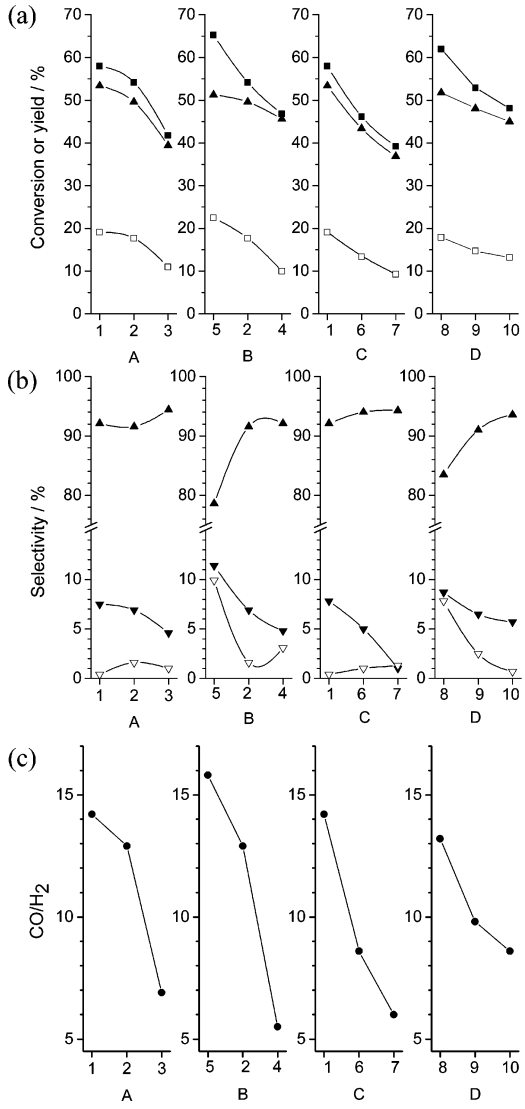

Figure 8. Catalytic activities of Cr−MSU-*x*: (a) ■ conversion of ethane, ▲ yield to ethylene, □ conversion of CO_2; (b) ▲ selectivity to ethylene, ▼ selectivity to methane, ▽ selectivity to CO; (c) ● molar ratio of CO/H_2 synthesized at different (A) initial Si/Cr ratios of Cr−MSU-1, (B) aging times, (C) aging temperatures, and (D) initial Si/Cr ratios of Cr−MSU-2 in the ODH of ethane with CO_2. The *x*-coordinate corresponds to the sample number, as specified in Table 1. Reaction conditions: $V(CO_2) = 9$ mL/min, $V(C_2H_6) = 3$ mL/min; catalyst load: 0.2 g; atmospheric: 700 °C.

(reaction 4) and the reforming reaction between ethane and CO_2 (reaction 5) act as the main side reactions, and methane and carbon monoxide are the main unexpected products converted from ethane. The conversion of ethane and CO_2, accompanied by a yield to ethylene, is shown in Figure 8a. The increase of the initial Si/Cr molar ratio in the precursor solution results in the reduction of Cr content in the final products and consequently the decline of ethane conversion on both Cr−MSU-1 (samples 1−3) and Cr−MSU-2 (samples 8−10). Similarly, shorter aging times in the synthesis lead to higher Cr contents in calcined catalyst samples and enhancement of ethane conversion (samples 2, 4, 5). Sample 5 synthesized with an aging time of 4 h gives the highest conversion to ethane (65.3%) in all samples. The Cr content in the product decreases significantly with the improvement of synthesis temperature, and thus the conversion to ethane drops rapidly (samples 1, 6, 7). The reason for the above results is that the quantity of active sites provided by Cr species directly depends on the actual Cr content in the catalyst. The yield to ethylene exhibits a trend similar to that of ethane conversion and comes near it because of the increasing selectivity to ethylene under specified conditions. Selectivity to ethylene, methane, and CO is shown in Figure 8b. As mentioned above, lower initial Si/Cr molar ratios, longer aging times, and higher aging temperatures result in lower Cr content, which consequently leads to a decrease in ethane conversion but an increase in selectivity to ethylene. With the increase of ethylene selectivity under the investigated conditions, the selectivity of methane, the main byproduct, drops quickly, indicating that the hydrogenolysis of ethane (reaction 4) is very restrained. Unlike methane, selectivity to CO shows a ruleless variation under investigation, but it always gives a lower value than methane selectivity. A lower selectivity to ethylene of less than 90% is present for samples 5 and 8. However, the highest conversions to ethane are also present for those two samples, suggesting that Cr species are also active for some side reactions at higher reaction temperatures. At the same time, it also reveals that the increase in reaction activity is at the expense of objective product selectivity. Figure 8c shows that the molar ratio of CO/H_2 in the product decreases under the investigated conditions, which should relate to the great drop in CO_2 conversion to CO under corresponding conditions.

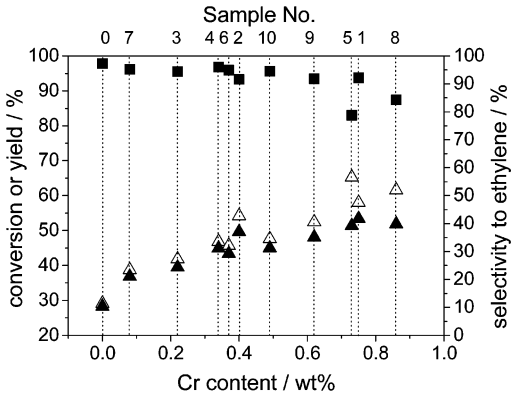

Figure 9. The correlation of the catalytic properties and Cr content of Cr−MSU-*x* in the dehydrogenation of ethane to ethylene with CO_2 at 700 °C: (△) conversion of ethane; (▲) yield to ethylene; (■) selectivity to ethylene.

The correlation of the catalytic properties of Cr−MSU-*x* catalysts with actual Cr content in the dehydrogenation of ethane to ethylene under CO_2 at 700 °C is plotted in Figure 9. The conversion of ethane and yield to ethylene exhibits an ascending trend but not a monotone increase with the raise of Cr content. Samples 1, 5, and 8 give the highest conversions of 58.0, 65.3, and 61.6% respectively, which should be attributed to their higher Cr content. Both framework and nonframework Cr species may contribute to their catalytic activities (H_2-TPR result). On the contrary, selectivity to ethylene shows a roughly descending trend. Interestingly, the sequence of ethane conversion is contrary to the sequence of area ratio between two reduction peaks of Cr species obtained from H_2-TPR for samples 1, 5, and 8 (see Table 2). It means that Cr species in the

TABLE 3: TOF Values of Four Selected Samples Calculated on the Basis of the Conversion of Ethane

	TOF (h^{-1})	
sample no.	600 °C	650 °C
1	69.9	110.0
5	83.8	129.1
8	66.8	111.7
9	79.2	130.4
Cr/SiO_2[a]	11.9−23.7	17.1−34.3

[a] The results were calculated using the data of ref 29.

framework interacting with support are more active according to the foregoing discussion. Therefore, sample 5 produces higher ethane conversion compared to that of samples 1 and 8. On the basis of the above results, the catalytic properties of Cr−MSU-*x* depend on not only Cr content but also the state of the Cr species in the catalyst. Wang et al. investigated the effect of Cr_2O_3 loading in a Cr_2O_3/SiO_2 system on the catalytic activity of the same reaction we explored. Ethane conversion increases to a maximum and then drops with the increase in Cr_2O_3 content, while ethylene selectivity shows little difference.[29] However, Mimura found that the increment of Cr content caused a sudden decrease in ethylene selectivity over Cr/H−ZSM-5 catalyst.[30] In our investigation, ethane conversion increases with the rise in Cr content and does not give an extremum all along because the highest Cr content is only 0.86 wt %, a very low Cr loading compared with the Cr_2O_3 supported catalysts cited above.[29,30] With this low Cr loading, it is reasonable that the Cr species in Cr−MSU-*x* are expected to be highly dispersed, close to 100%.[28] On the basis of this hypothesis, the turnover frequency (TOF) values of some of the catalysts are calculated and listed in Table 3. Because the contributions of support and the homogeneous reaction to activity (ethane conversion) of catalysts with lower Cr contents have a significant effect on their TOF calculation results, four catalysts with relatively higher Cr contents (samples 1, 5, 8, and 9) are selected to calculate for more accurate results. For comparison, the TOF value of the conventional catalyst Cr_2O_3/SiO_2 is also calculated referenced to Wang's investigation.[29] Because of the formation of Cr_2O_3 crystallites on the surface of the SiO_2 support, whole Cr should not fully disperse as high as 100%. Therefore, the calculation of the TOF of Cr_2O_3/SiO_2 was performed on the hypothesis of 40−80% Cr dispersion, a wide range to include all possible results. From Table 3, the TOF values of the four selected samples exhibit equal levels at both 600 and 650 °C, and they outclass the TOF of Cr_2O_3/SiO_2 with ratios from 3.0:1 to 7.6:1 (TOF(Cr−MSU-*x*)/TOF(Cr/SiO_2)), indicating that Cr species on mesoporous Cr−MSU-*x* are more efficient than those on Cr/SiO_2 catalyst for the activation and conversion of ethane molecules. The outstanding performances of Cr−MSU-*x* should contribute to the high dispersion of Cr species on the channel wall and surface due to high area surface, the high oxidation state due to low Cr loading, and the unique redox ability due to the special mesostructure of the catalysts prepared.

Contrary to conventional reported chromium-supported catalysts,[4] we suppose that highly oxidized Cr^{6+} (or Cr^{5+}), not Cr^{3+} or Cr^{2+}, are the active species on Cr−MSU-*x* catalysts in the dehydrogenation of ethane with CO_2. It has been a general consensus that chromate and less oxidized polychromate (Cr^{6+} and traces of Cr^{5+}) are formed on the surface of supported chromium catalysts at a loading of about 1 wt % Cr oxide or less.[4] The above DR UV−vis and Cr K-edge XANES results have also proved that Cr(VI) with tetrahedral coordination is the main local structure of the Cr species in Cr−MSU-*x* samples. Wang et al. found that Cr(VI) in tetrahedral coordination formed as monochromate species in Cr−MCM-41 prepared by direct hydrothermal synthesis.[22,23] Sakthivel discovered that chromium was present as both Cr(V) and Cr(VI) in tetrahedral coordination in Cr−MCM-41 by DR UV−vis and electron paramagnetic resonance characterization.[31] The reduction of Cr^{6+} was observed in our H_2-TPR study. In summary, the highly valent Cr species (Cr^{6+} and traces of Cr^{5+}) should be responsible for the catalytic activities of Cr−MSU-*x* in the dehydrogenation of ethane with CO_2 as we investigated. The stability of Cr−MSU-*x* in the dehydrogenation of ethane to ethylene under CO_2 was also investigated, and it was presented in detail in our previous paper.[32] A decrease in ethane conversion from 50.1 to 37.6% in 3 h under the specified conditions was observed. At the same time, a reduction of highly valent Cr species was also detected in the reaction. Therefore, the highly valent Cr species were expected to be active sites, and the reduction of these Cr species acted as one main reason for the deactivation of Cr−MSU-1 catalyst in the investigated reaction.

Conclusions

Synthesis parameters, including different templates, initial Si/Cr molar ratios, aging times, and temperature, have a detectable influence on the actual Cr content and structure property of mesoporous chromium-incorporated MSU-*x* molecular sieves that were prepared by nonionic PEO surfactant templating under acidic conditions. Higher concentrations of chromium in the source gel solution, shorter aging times, and lower aging temperatures could increase the actual Cr content but reduce the short-range order of the Cr−MSU-*x* product. DR UV−vis and XANES spectra show that tetrahedrally substituted chromium atoms are induced to Cr−MSU-*x*. Two kinds of Cr^{6+} species with different reduction abilities were found in the TPR study. Cr−MSU-*x* exhibits good catalytic activity in the oxidative dehydrogenation of ethane to ethylene with CO_2. The actual Cr content and structure property, which depend on the synthesis conditions, strongly affect the catalytic capability of Cr−MSU-*x* in the reaction.

Acknowledgment. The authors are grateful for the financial support of the National Science Foundation of China (Grant No. 20436050) and the National 863 Program Youth Foundation of China (Grant No. 2004AA649230).

References and Notes

(1) Stephen, A. B.; Tim, K.; Milestone, N. B. *Microporous Mesoporous Mater.* **1998**, *22*, 419.
(2) Vinu, A.; Srinivasu, P.; Miyahara, M.; Ariga, K. *J. Phys. Chem. B* **2006**, *110*, 801.
(3) Trong, O. D.; Desplantier, G. D.; Danumah, C.; Kaliaguine, S. *Appl. Catal., A* **2003**, *253*, 545.
(4) Weckhuysen, B. M.; Schoonheydt, R. A. *Catal. Today* **1999**, *51*, 223.
(5) Bagshaw, S. A.; Prouzet, E.; Pinnavaia, T. J. *Science* **1995**, *269*, 1242.
(6) Sierra, L.; Guth, J. L. *Microporous Mesoporous Mater.* **1999**, *27*, 243.
(7) Liu, L.; Li, H.; Cai, W.; Zhang, Y. *Acta Phys.−Chim. Sin.* **2005**, *21*, 1311.
(8) Chen, Y.; Huang, Y.; Xiu, J.; Han, X.; Bao, X. *Appl. Catal., A* **2004**, *273*, 185.
(9) Melero, J.; Arsuaga, J.; de Frutos, P.; Iglesias, J.; Sainz, J.; Blázquez, S. *Microporous Mesoporous Mater.* **2005**, *86*, 364.
(10) Arnold, A. B. J.; Niederer, J. P. M.; Niessen, T. E. W.; Hölderich, W. F. *Microporous Mesoporous Mater.* **1999**, *28*, 353.
(11) Chao, M.; Lin, H.; Wang, D.; Tang, C. *Microporous Mesoporous Mater.* **2005**, *83*, 269.
(12) Li, Y.; Yang, J.; Tang, Y.; Bai, L.; Xiang, H.; Li, Y. *J. Fuel Chem. Technol.* **2003**, *31*, 171.

(13) Reddy, K. R.; Ramaswamy, A. V.; Ratnasamy, P. *J. Catal.* **1993**, *134*, 275.
(14) Reddy, K. M.; Moudrakovski, I.; Sayari, A. *J. Chem. Soc., Chem. Commun.* **1994**, 1059.
(15) Parvulescu, V.; Anastasescu, C.; Su, B. L. *J. Mol. Catal. A.* **2004**, *211*, 143.
(16) Zhai, S.; Wei, W.; Wu, D.; Sun, Y. *Catal. Lett.* **2003**, *89*, 261.
(17) Yu, J.; Li, C.; Xu, L.; Li, M.; Xin, Q. Liu, Z. *Chin. J. Catal.* **2001**, *22*, 331.
(18) Brunauer, S.; Deming, L. S.; Deming, W. E.; Teller, E. *J. Am. Chem. Soc.* **1940**, *62*, 1723.
(19) Jiménez-López, A.; Rodríguez-Castellón, E.; Maireles-Torres, P.; Díaz, L.; Mérida-Robles, J. *Appl. Catal., A* **2001**, *218*, 295.
(20) Yuan, Z.; Wang, J.; Zhang, Z.; Chen, T.; Li, H. *Microporous Mesoporous Mater.* **2001**, *43*, 227.
(21) Kustrowski, P.; Chmielarz, L.; Dziembaj, R.; Cool, P.; Vansant, E. F. *J. Phys. Chem. B* **2005**, *109*, 11552.
(22) Wang, Y.; Ohishi, Y.; Shishido, T.; Zhang, Q. H.; Yang, W.; Guo, Q.; Wan, H. L.; Takehira, K. *J. Catal.* **2003**, *220*, 347.
(23) Takehira, K.; Ohishi, Y.; Shishido, T.; Kawabata, T.; Takaki, K.; Zhang, Q. H.; Wang, Y. *J. Catal.* **2004**, *224*, 404.
(24) Requejo, F. G.; Ramallo-López, J. M.; Rosas-Salas, R.; Domínguez, J. M.; Rodriguez, J. A.; Kim, J.-Y.; Quijada, R. *Catal. Today* **2005**, *107*−*108*, 750.
(25) Gardea-Torresdey, J. L.; Tiemann, K. J.; Armendariz, V.; Bess-Oberto, L.; Chianelli, R. R.; Rios, J.; Parsons, J. G.; Gamez, G. *J. Hazard. Mater. B* **2000**, *80*, 175.
(26) Wei, Y. L.; Lee, Y. C.; Hsieh, H. F. *Chemosphere* **2005**, *61*, 1051.
(27) Balasubramanian, M.; Melendres, C. A. *Electrochim. Acta* **1999**, *44*, 2941.
(28) Yim, S. D.; Nam, I.-S. *J. Catal.* **2004**, *221*, 601.
(29) Wang, S. B.; Murata, K.; Hayakawa, T.; Hamakawa, S.; Suzuki, K. *Appl. Catal., A* **2000**, *196*, 1.
(30) Mimura, N.; Takahara, I.; Inaba, M.; Okamoto, M.; Murata, K. *Catal. Commun.* **2002**, *3*, 257.
(31) Sakthivel, A.; Selvam, P. *J. Catal.* **2002**, *211*, 134.
(32) Liu, L. C.; Li, H. Q.; Zhang, Y. *Catal. Today* **2006**, *115*, 235.